

# *A Final Report for*

## Source Location Determination of Uranian Kilometric Radiation From Ray Tracing and Emission Lobe Modelling

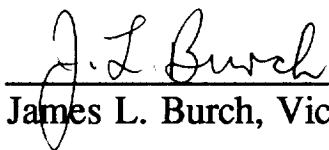
Principal Investigator:

J.D. Menietti  
Southwest Research Institute  
P.O. Drawer 28510  
San Antonio, TX 78228-0510  
(512) 522-3210

Submitted To:

Jet Propulsion Laboratories  
JPL No. 958828  
September 1991

Approval:

  
James L. Burch, Vice President



### SOUTHWEST RESEARCH INSTITUTE

Instrumentation and Space Research Division  
6220 Culebra Road, San Antonio, Texas 78228-0510  
(512) 684-5111 • (512) 647-4325

This report was prepared for the Jet Propulsion Laboratory,  
California Institute of Technology, sponsored by the  
National Aeronautics and Space Administration.

# Source Location Determination of Uranian Kilometric Radiation From Ray Tracing and Emission Lobe Modelling

ORIGINAL CONTENTS

## Abstract

COLOR ILLUSTRATIONS

We use an analytical fit to an emission lobe profile together with three-dimensional ray tracing to model the broad-banded smooth Uranian kilometric radiation (UKR). We assume the radiation is gyroemission from sources along magnetic field lines. Using an iterative technique that modifies the lobe function and source region, the results are compared to observations at a frequency of 481 kHz. The best-fit calculations are compared to previously published models and to recent UV observations.

## 1. Introduction

Since the initial observation of broadband Uranian kilometric radiation (UKR) in the frequency range  $20 \text{ kHz} < f < 900 \text{ kHz}$  by the Planetary Radio Astronomy (PRA) instrument on board the Voyager 2 spacecraft [Warwick et al., 1986], numerous authors have suggested source locations for the emission (see the special Voyager issue of *Journal of Geophysical Research*, December 1987). These models were constructed by assuming straight-line propagation from the source region, and assuming the offset tilted dipole (OTD) magnetic field model [Ness et al., 1986]. The number and diversity of the proposed source regions indicates the lack of consensus regarding the UKR emissions.

Besides the discrepancy in the source location, there is also disagreement regarding the shape of the emission cone or radiation lobe. Most authors suggest that it is some form of a hollow emission cone to explain the periodic decrease in higher-frequency intensity that is called the "bite-out" by Warwick et al. [1986], but there is little agreement on the precise shape of the beaming pattern.

In addition to the bite-out, another feature of the Voyager observations that deserves attention is the rather abrupt detection of first the lower then higher frequencies shortly after closest approach. It is possible that these two features originate from separate source regions. Gulkis and Carr [1987] have used an empirical fit to an emission lobe to obtain a reasonably good fits to the general profile of data extended over many days. More recently, Menietti et al. [1990] have performed a ray tracing study incorporating the Q-3 magnetic field model [Connerney et al., 1987] and shown that the source region of the UKR must be extended in longitude to explain both the bite-out in the emission spectra observed for frequencies,  $f \geq 400 \text{ kHz}$  and the observations near closest approach (CA).

In this paper we have performed a ray tracing study assuming a lobe emission profile that is constrained by the observations at a frequency of 481 kHz. By varying both the emission lobe shape and the assumed source region we obtain a best-fit model. We compare our results to model fits of the UV emission intensity near the cloud tops [Herbert and Sandel 1990].

## 2. Models and Approach

The magnetic field incorporated in this study is the Q-3 model of Connerney et al. [1987]. The plasma model for  $r > 4.2 r_U$  (CA) is an empirical fit to the data as published by McNutt et al. [1987] and Sittler et al. [1987]. For  $r < 4.2 r_U$ , we have chosen a three-parameter fit to an exponential as defined in Menietti et al., p. 53 [1990]. We assume Doppler-shifted gyroemission with sources along the magnetic field line. By simultaneously solving the cold plasma dispersion relation and the condition for gyroresonance we have determined that the ratio of wave frequency to the RX cutoff frequency,  $f/f_{RX} = 1.03$ , is reasonable for a ratio of plasma frequency to gyrofrequency,  $f_p/f_g < 0.3$ , energies  $E < 20$  keV, and for wave normal angles in the range  $90^\circ < \Psi < 130^\circ$ . The beam profile or lobe function used in this study was introduced by Gulkis and Carr [1987] as

$$f(\Psi) = I_o \left\{ \frac{1}{2} + \frac{1}{2} \cos[n(\Psi - \Psi_o)] \right\} \quad (1)$$

where  $f(\Psi)$  is the relative power per unit solid angle radiated in the direction making an angle  $\Psi$  with the negative direction of the B-vector at the source;  $\Psi_o$  is the emission cone half-angle; and  $n$  is a parameter that determines the beam thickness.

The procedure for fitting the intensity versus time profile of the emission at a given frequency begins by defining a specific region on the Uranian surface that represents the region of footprints of magnetic field lines along which sources of UKR exist. We assume that each source within this region emits at the same intensity,  $I_o$ . If we define  $d_{ji}$  as the distance between the source at position  $j$  and spacecraft at time  $t_i$ , then the calculated intensity measured by the spacecraft is

$$I(t_i) = \sum_j f(\Psi_j, k_{ji}, n, \Psi_o) \quad (2)$$

$\Psi_j$  is determined from the ray tracing results and is the calculated wave normal angle of the emission that actually intercepts the spacecraft. This is obtained by superimposing the spacecraft position on plots of the intersection of the emission cone at specific times (or equivalently at different spacecraft distances). The emission cones are generated by launching the rays at specific initial wave normal angles in 18 different azimuth angles around each "active" magnetic field line. We consider 3 different initial wave normal angles,  $\Psi_o$ , for each source point, and each group of rays at constant  $\Psi_o$  produces a unique emission cone as observed at a specific spacecraft time. In Figure 1 we show a typical plot of the spacecraft position superimposed on the emission cones for a specific source point. From this plot we obtain the value of  $\Psi_j$ . Tables are then constructed of values of  $\Psi_j$  for each source position considered within a specified source region. During the fitting process, for a given source region we vary the parameters  $n$  and  $\Psi_o$  in equation 2 until the profile of  $I(t)$  best matches the observations as determined by minimizing  $\chi^2$ .

We have created a grid in Uranocentric longitude and latitude with the footprint of field lines containing source points located in the center of boxes  $4^\circ \times 4^\circ$  for the nightside. Figure 12 of Menietti et al. [1990] summarizes the source locations of UKR as determined from a number of different authors. The source locations were determined using the OTD magnetic field model. Even though the present study assumes the Q-3 magnetic field model, we have nevertheless used the candidate source locations depicted in the figure as appropriate "first estimates". We approximate the source locations as best as we can using the  $4^\circ \times 4^\circ$  resolution of the ray tracing results. We then varied the shape of each estimated source location until we obtained a best fit to the data. In Figures 2 and 3 we indicate the candidate source locations considered for presentation.

### 3. Results

We present the results of the study in the form of calculated values of intensity for 24 different times (or spacecraft positions) superimposed on the actual data for a frequency of 481 kHz. We have chosen this frequency because it clearly depicts the bite-out feature. The figures chosen for presentation summarize the essential or salient findings of our study. We have chosen two distinct time periods for which to compare the calculated intensities to the observations: the period near CA on day 24 of 1987 around 18 hours; and the period near the first observation of a large bite-out at the higher frequencies, centered approximately around 16 hours of day 25. We consider first the region near CA in Figure 4. The calculated values of intensity are indicated with asterisks, and the source region is G1. Please note that the emission observed near 15:30 is broadbanded bursty emission and was not considered in the fitting process. For this source region, the emission lobe parameters for equation 1 that best fit the intensity profile of  $I(t)$  are indicated on the figure as  $\Psi_o = 25^\circ$  and  $n=2$ . It is clear that a reasonable fit is obtained for time  $\geq 20$  hours, but the data near CA is poorly fit. The spacecraft for these times simply does not see the emission. This same general result was also obtained for source regions Z and K3 even though the best-fit parameters varied somewhat. For these sources, the data can only be fitted for times  $t \geq 20$  hours. In Figure 5, however, we note that the calculated intensities fit the data rather well for the source region designated L2, for the fitting parameters  $\Psi_o=43^\circ$  and  $n=3$ .

We next consider the first wide bite-out observed in the data. In Figure 6 we note that the calculated intensities can only be fit to one side of the bite-out for the source region labelled Z. A similar result occurred for the source region labelled K3. However, in Figures 7a and 7b we note that the source region labelled G1 can produce a reasonable fit for fitting parameters of  $\Psi_o=50^\circ$ ,  $n=4$  or  $\Psi_o=47^\circ$ ,  $n=8$ . Finally we consider the source region designated A, which we found gave us the best fit to the data both near CA and for the bite-out. In Figure 8a the fit to the bite-out region for source location A is respectable, but the fit to the region near CA (Fig. 8b) shows some points that still fall below the data. Another "problem" with the latter fit is that the fitting parameters are somewhat anomalous, because the emission lobe is fatter and more field aligned than in the any of the other cases. We summarize the results of the calculations and emission lobes in Table 1.

**Table 1**  
**Best Fit Results of the Ray Tracing Calculations**

Source Region	Data Region	Fitting Parameters	
		$\Psi_0$	n
L2	CA	43°	3
G1	bite-out	47°	4-8
A	CA	25°	2
A	bite-out	50°	4.5

#### 4. Comparison With UV Emissions

Herbert and Sandel [1990] have presented contours of the UV emission from Uranus near the cloud tops as determined from spherical harmonic fits of the spectral data. Such emission is likely due to precipitating electrons which are in turn probable free-energy sources for the UKR. For this reason we have superimposed the regions considered in this study on a plot of the UV emission as seen in Figure 9. It is evident that some of the regions match the intense "hot spot" near the south magnetic pole. This agreement suggests that the assumptions for the generation of the calculated intensities are reasonable.

#### 5. Summary

In this study we have presented the results of ray tracing of UKR with a model emission lobe. The source region of the emission and the emission lobe shape were both varied until the calculated intensity best matched the actual data. This study differs from that performed previously by Gulkis and Carr [1987] because ray tracing has been incorporated and because the data was fit at higher resolution than in the work of Gulkis and Carr. We conclude from this study that

- 1) The source region of nightside UKR appears to be extended in longitude in order to explain both the bite-out and the emission near CA.
- 2) The emission lobe appears to be best fit with the maximum power at  $\Psi_0 \sim 45^\circ$  and with a beam width in the range of about  $25^\circ$  to  $65^\circ$ .

- 3) Temporal effects may be necessary to explain the emission near CA because no one source region adequately fit the data both near CA and the bite-out.
- 4) The source region indicated by the ray tracing overlaps the region of the UV enhancement near the south magnetic pole. This suggests that the free-energy source of the UKR also generates the UV emission.

It is also important to note that we have assumed that  $I_0$  is a constant over the entire source region. This approximation is no doubt incorrect, but to assume anything else would introduce too many fitting parameters and make the problem intractable. As suggested in point 3 above, either a time or a spatial dependence of  $I_0$  could account for the lack of adequate fitting of region A to the data in both the region near CA and the bite-out.

**Acknowledgments.** We gratefully recognize G. Perez for clerical assistance and Tony Sawka for drafting of the figures. This work was supported by NASA grant NAGW-1205 and by a JPL subcontract to SwRI, 15-3679 (JPL 958828).

## 6. References

- Connerney, J.E.P.; M.H. Acuna, N.F. Ness: The Magnetic Field of Uranus, *J. Geophys. Res.*, **92**, 15329, 1987.
- Gulkis, S. and T. D. Carr, The Main Source of Radio Emission From the Magnetosphere of Uranus, *J. Geophys. Res.*, **92**, 15159, 1987.
- Herbert, Floyd and B. R. Sandel, The Uranian Aurora, abstract presented at the Fred Scarf Memorial Symposium on Magnetospheres of the Outer Planets, Annapolis, MD, August 20-24, 1990.
- McNutt, R. L., Jr., R. S. Selesnick, and J. D. Richardson, Low-energy plasma observations in the magnetosphere of Uranus *J. Geophys. Res.*, **92**, 4399, 1987.
- Menietti, J. D., H.K. Wong, D.A. Wah, and C.S. Lin, Source Region of the Smooth High Frequency Nightside Uranus Kilometric Radiation, *J. Geophys. Res.*, **95**, 51, 1990a.
- Ness, N.F., M.H. Acuna, K.W. Behannon, L.F. Burlaga, J.E.P. Connerney, R.P. Lepping, and F.M. Neubauer, Magnetic Fields at Uranus, *Science*, **233**, 85, 1986.
- Sittler, E. C. Jr., K. W. Ogilvie, and R. Selesnick, Survey of electrons in the Uranian magnetosphere: Voyager 2 observations, *J. Geophys. Res.*, **92**, 15263, 1987.

## 7. Figure Captions

Figure 1. This is an example of the intersection of the emission cone for three different initial wave normal angles  $\Psi$  with a spherical shell at a radius of  $15.7 r_U$ . The angle  $\theta$  is measured from the uranocentric z axis;  $\phi$  is the azimuthal angle.

Figure 2. Regions on the surface of Uranus containing footprints of magnetic field lines that were sampled as source field lines for the ray-tracing calculations. The footprints are located in the center of boxes  $4^\circ \times 4^\circ$ . The plot is displayed in uranocentric coordinates.

Figure 3. Same as Figure 2.

Figure 4. The solid curve is the observed intensity (arbitrary units) versus time for the radio emission at a frequency of 481 kHz. The calculated intensity values are shown as asterisks. The assumed source region was G1 and the parameters of equation 1 that produced the best fit are also indicated. Note that the b-bursty emission was not considered in the fitting scheme.

Figure 5. Same as Figure 4 except for source region L2

Figure 6. This is a comparison of the intensity of the radio emission to the calculated values during times when the bite-out was observed. The assumed source region was Z.

Figure 7. Same as Figure 6 but now for source region G1. The fit for the narrower emission cone ( $n=8$ ) shown in the bottom panel (7b) is perhaps somewhat better than that of the wider emission cone ( $n=4$ ) shown in the top panel (7a).

Figure 8. The format is the same as in previous figures. Here we display the results of using the same source region (A) to fit the emission observed at times when the bite-out was observed (top), and at times near CA.

Figure 9. This is a color contour (uranocentric coordinates) of auroral UV intensity at Uranus. The plot is produced by linear combinations of spherical harmonics to 8th order, fit by the singular value decomposition inversion technique [cf. Connerney et al., 1987]. The color bar is along the left edge with white the most intense. Superimposed in black on the UV color contours are the source locations considered in this study. Note that all of the regions lie close to the auroral "hot spot" near the south magnetic pole.

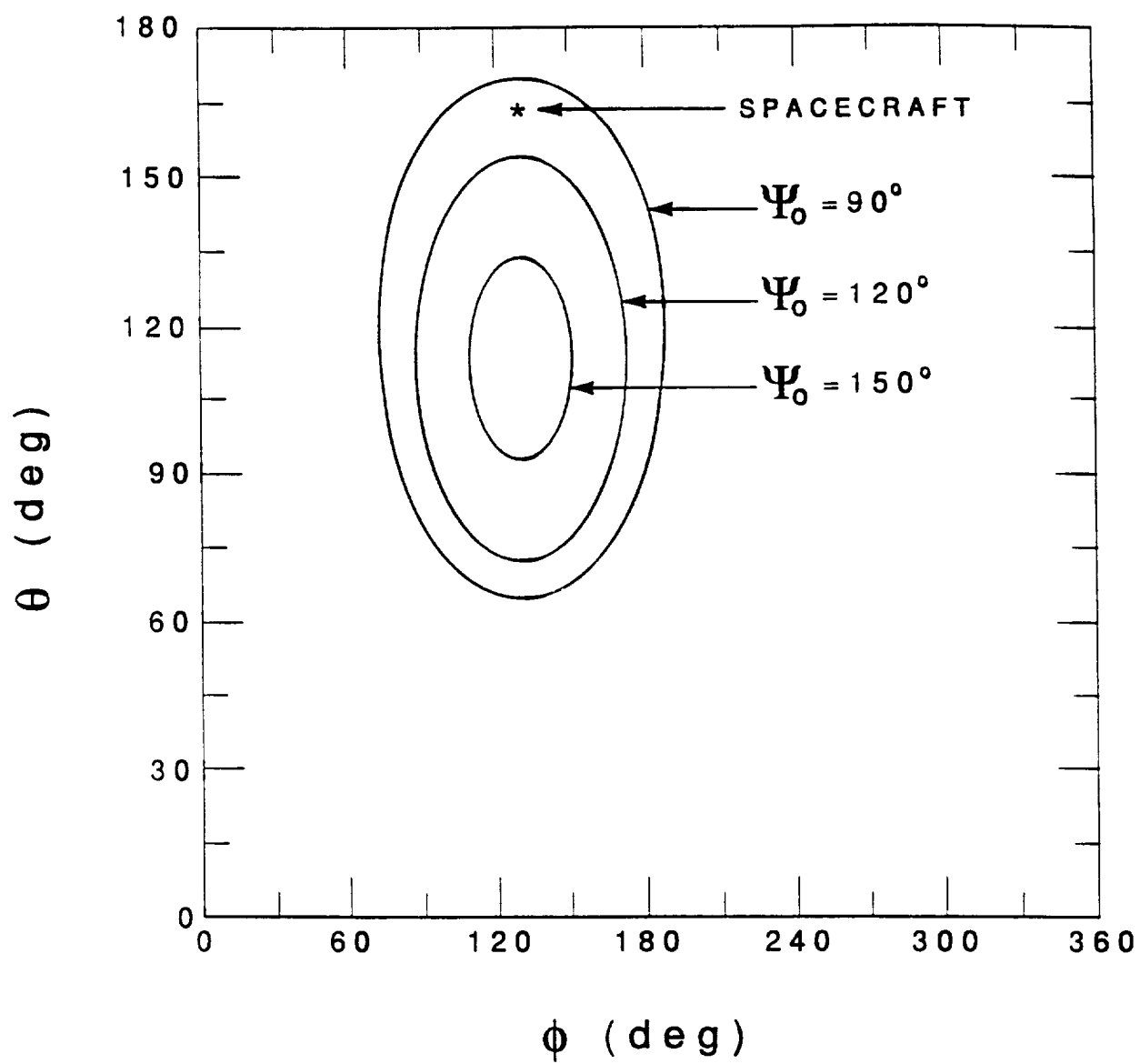


Figure 1



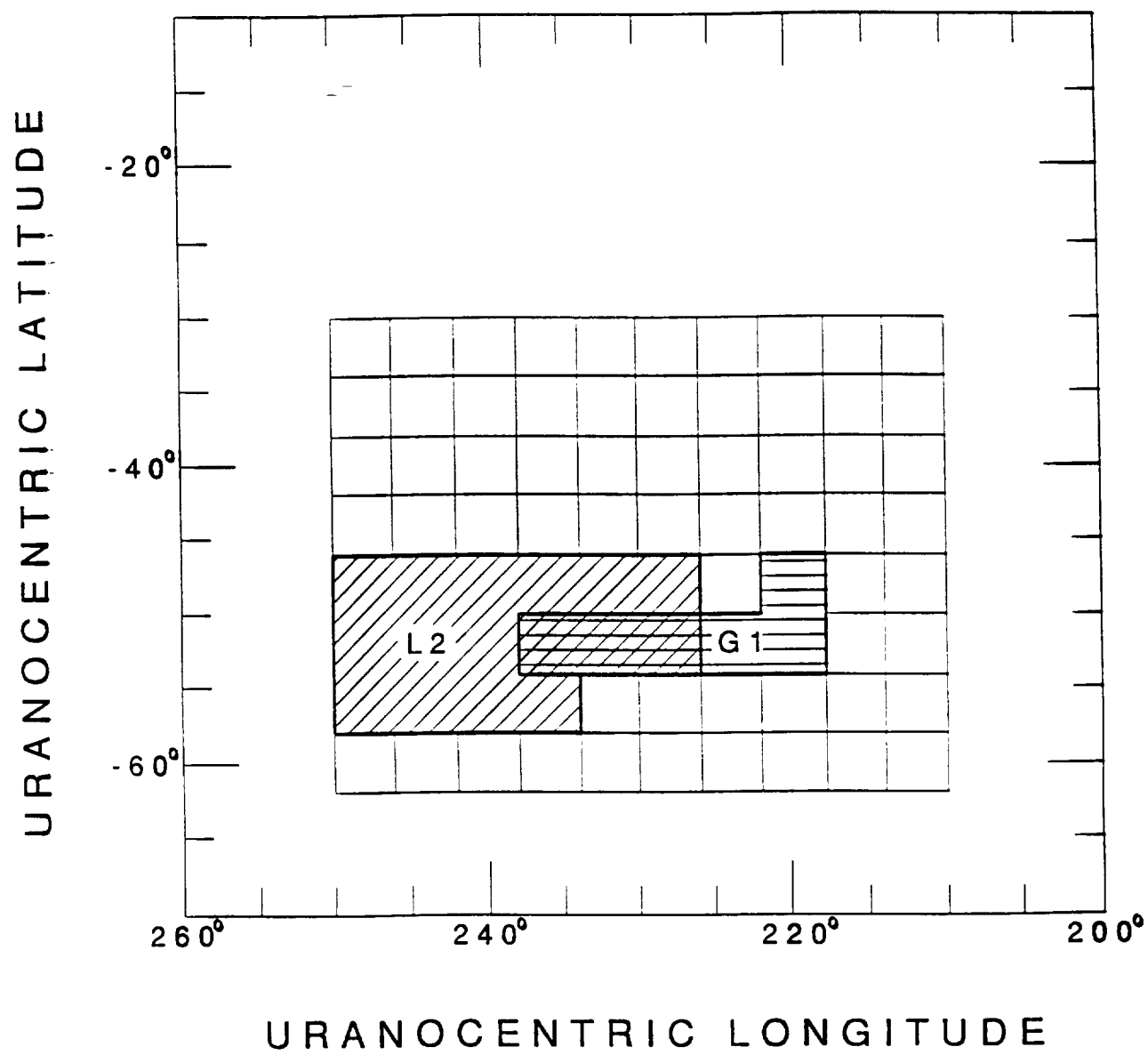


Figure 2

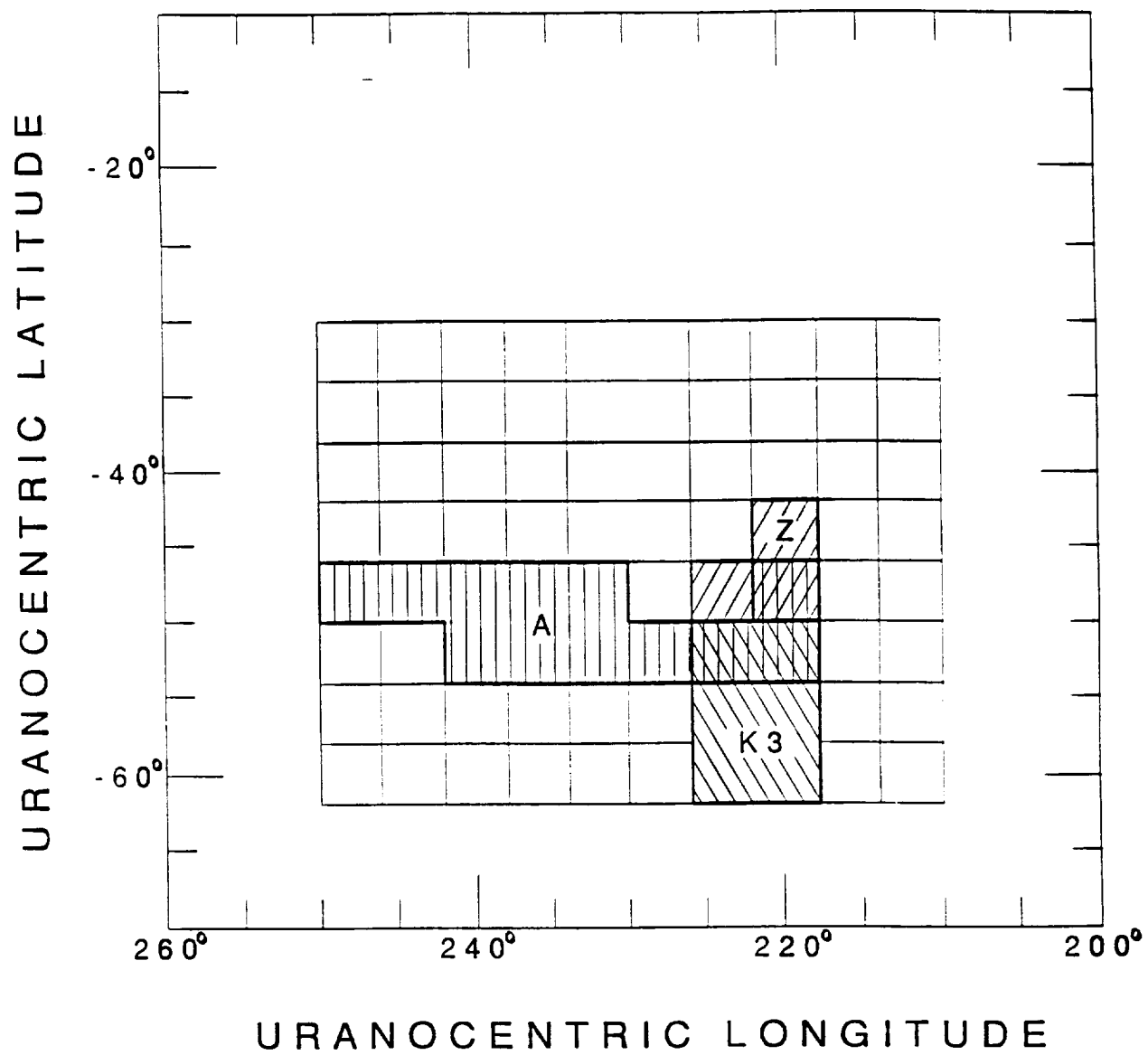


Figure 3

INTENSITY vs TIME (LEFT POLAR)  
VOYAGER 2 860124 8 01 00 TO 8 59 00  
FREQUENCY 481 KHZ

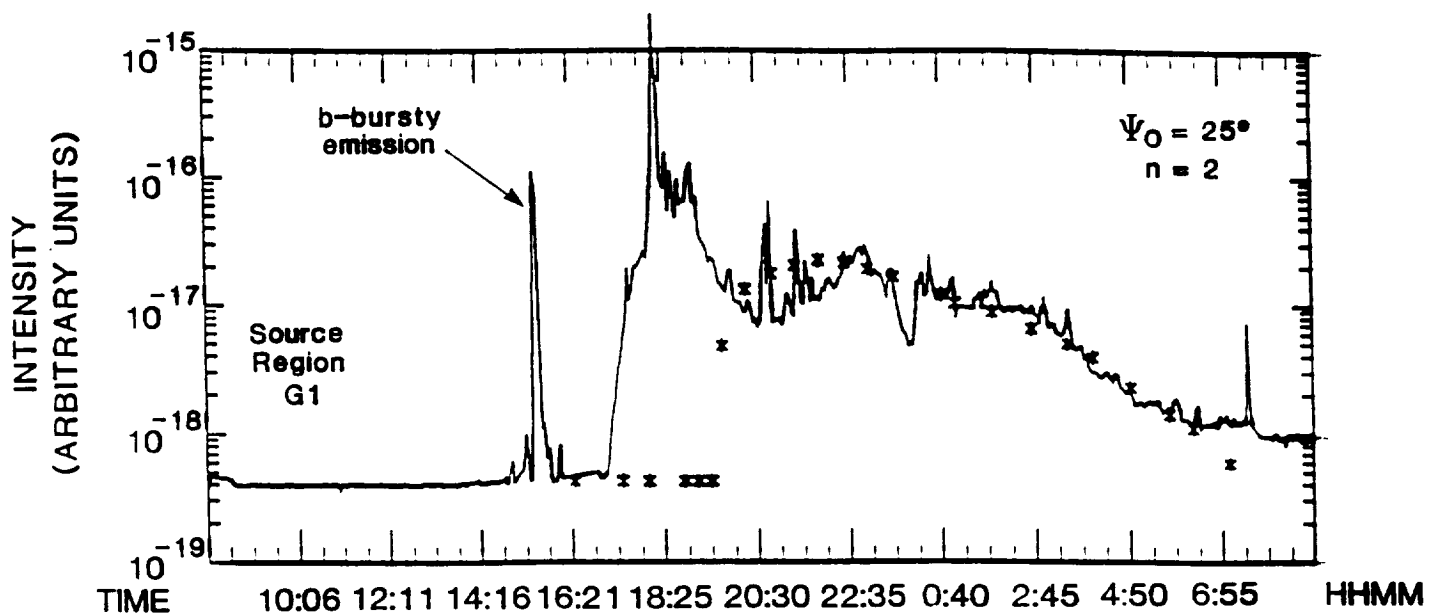


Figure 4

INTENSITY vs TIME (LEFT POLAR)  
VOYAGER 2 860124 8 01 00 TO 8 59 00  
FREQUENCY 481 KHZ

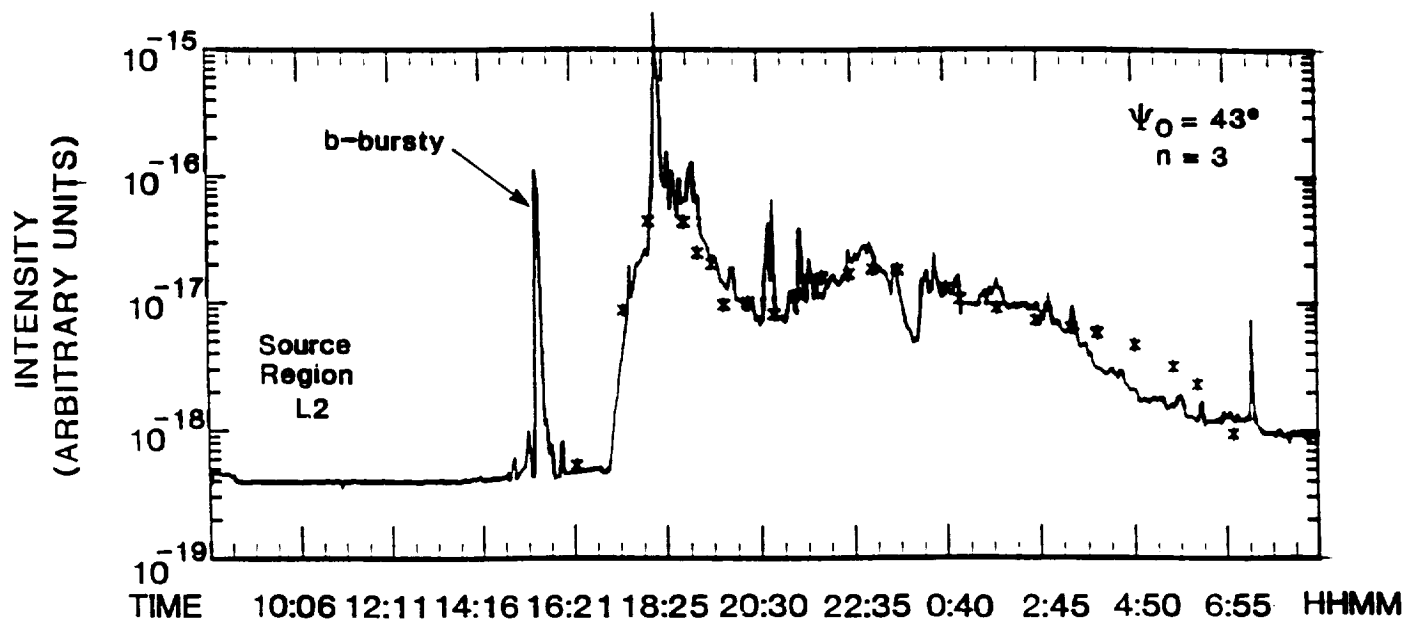


Figure 5

INTENSITY vs TIME (LEFT POLAR)  
VOYAGER 2 860125 11 01 00 TO 23 58 00  
FREQUENCY 481 KHZ

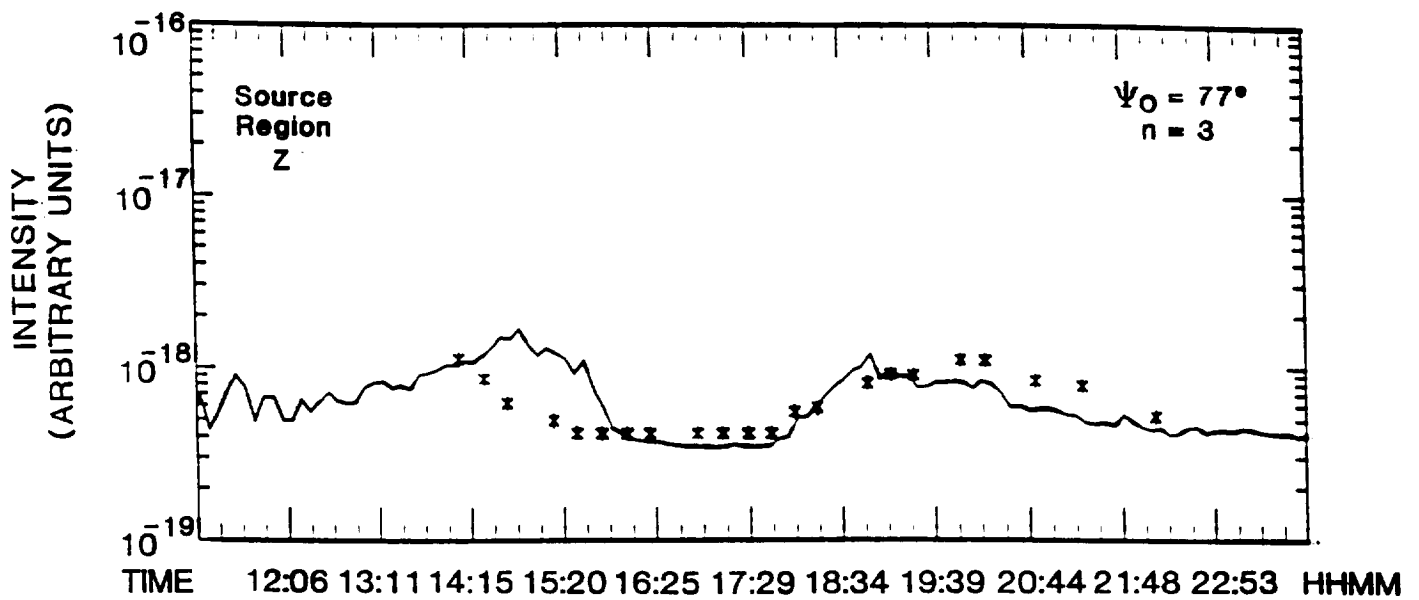


Figure 6

# INTENSITY vs TIME (LEFT POLAR)

VOYAGER 2 860125 11 01 00 TO 23 58 00

FREQUENCY 481 KHZ

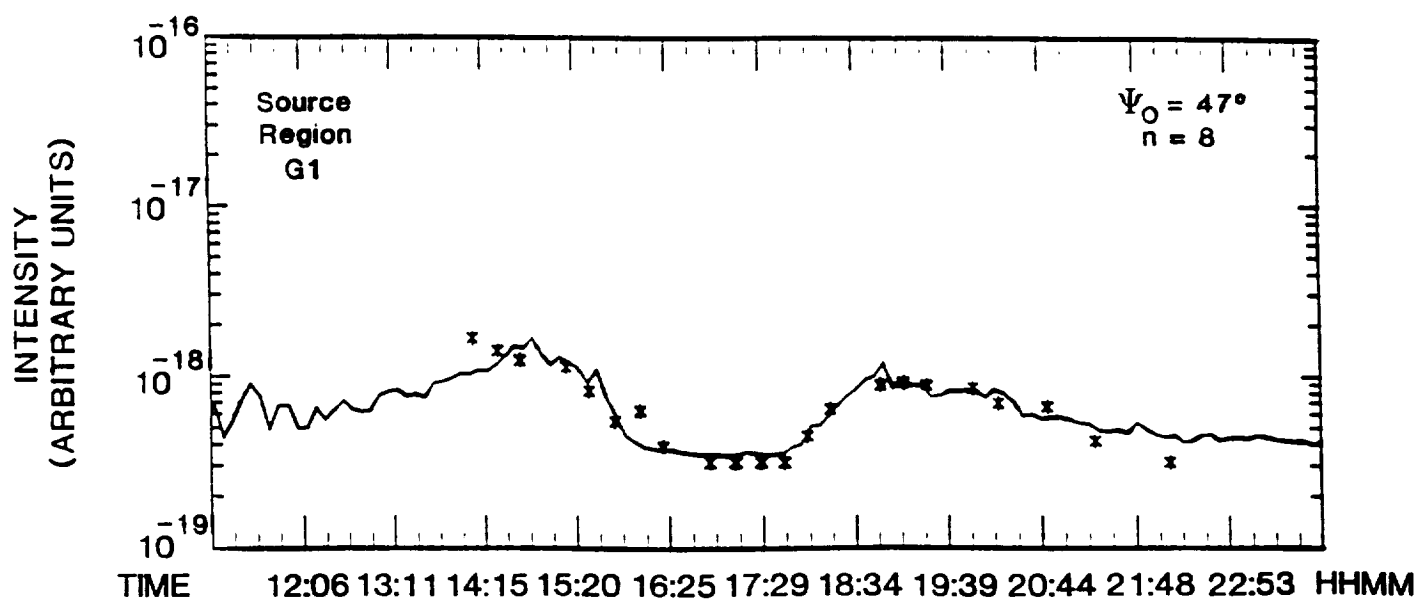
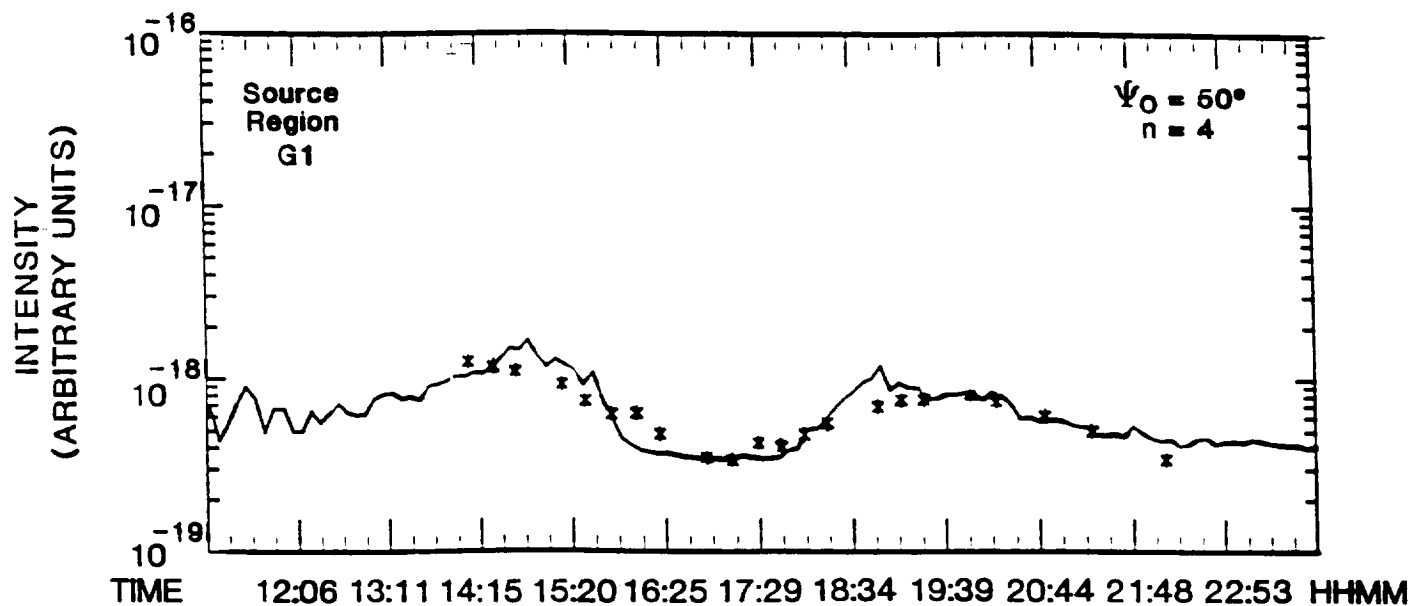


Figure 7a,b

# INTENSITY vs TIME (LEFT POLAR)

VOYAGER 2 860125 11 01 00 TO 23 58 00

FREQUENCY 481 KHZ

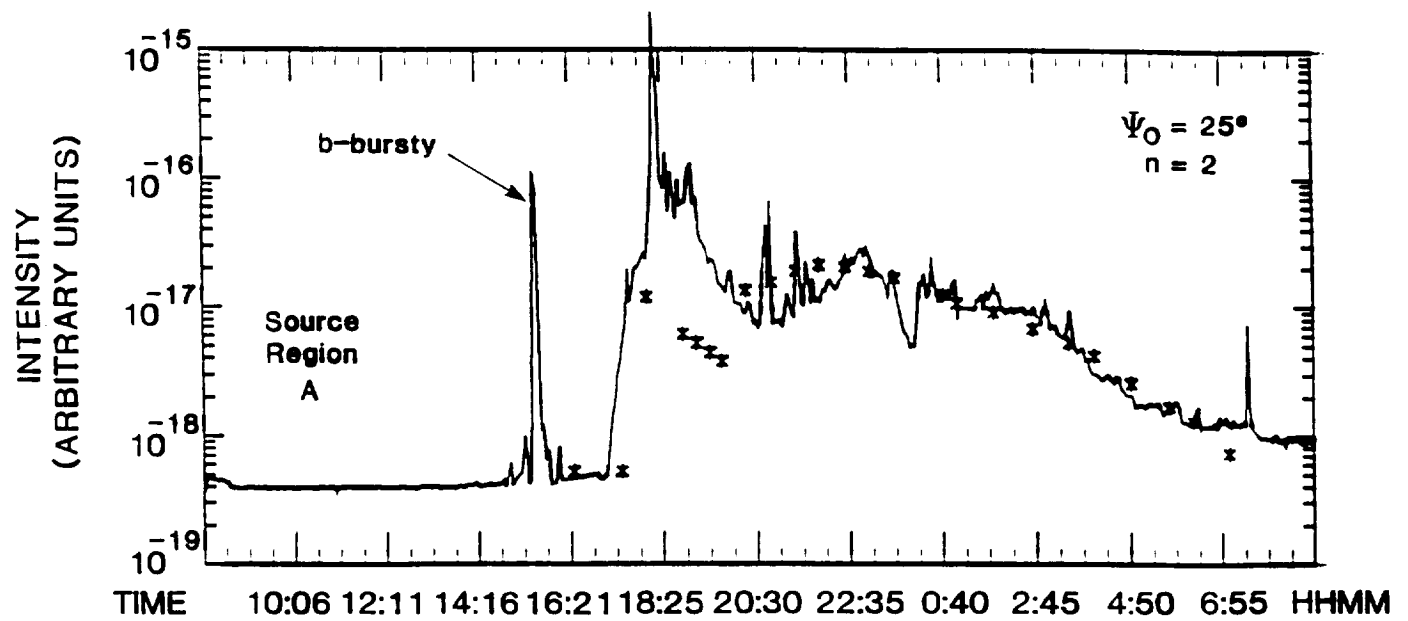
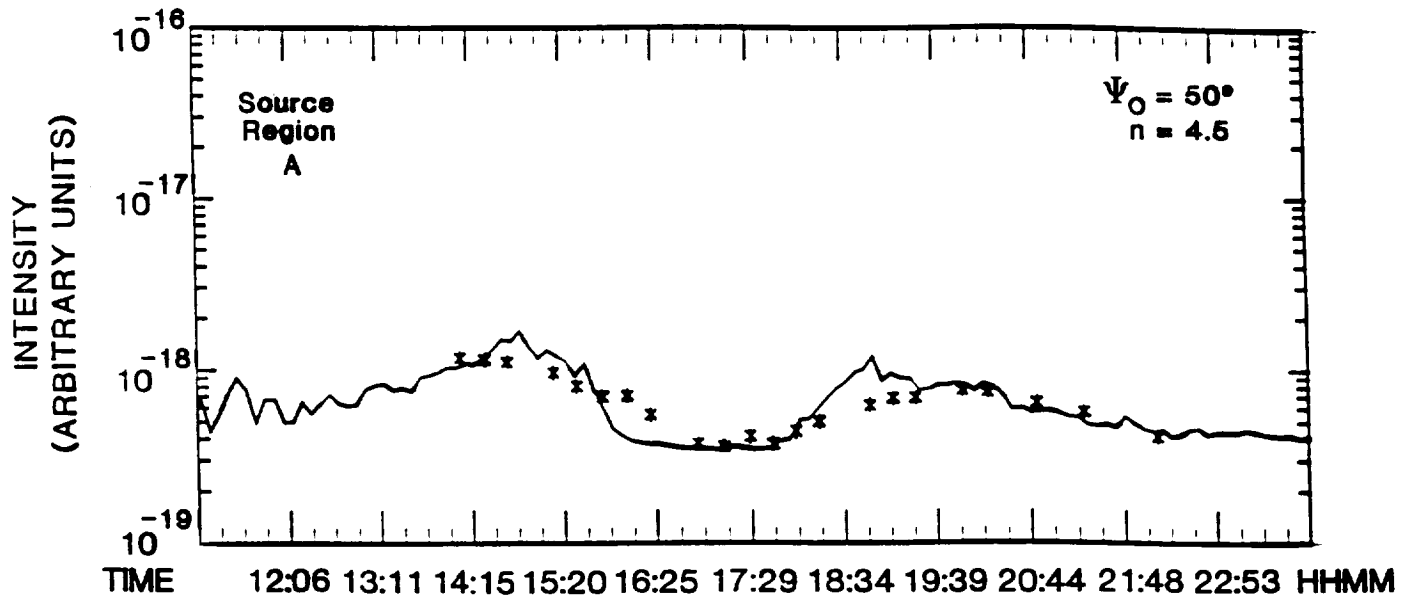


Figure 8a,b

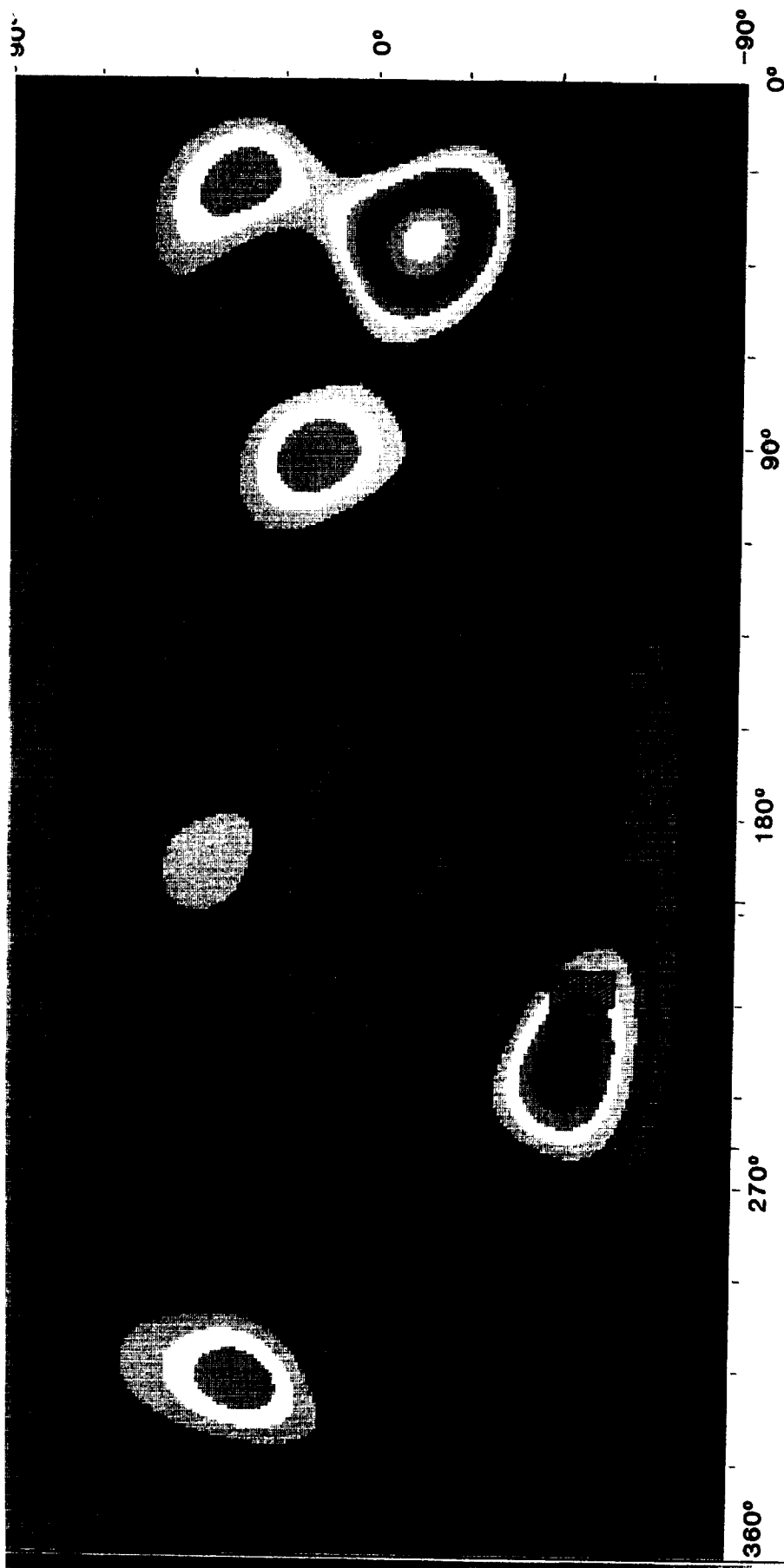


Figure 9